A pragmatic approach to abstract the excavation damaged zone around tunnels of a geological radioactive waste repository: application to the HG-A experiment in Mont Terri

ANDRÉS ALCOLEA[1]*, ULI KUHLMANN[1], PAUL MARSCHALL[2], ANDREA LISJAK[3], GIOVANNI GRASSELLI[3], OMID MAHABADI[3], RÉMI DE LA VAISSIÈRE[4], HELEN LEUNG[5] & HUA SHAO[6]

[1]*TK Consult AG, Hallenstrasse 10, 8008 Zürich, Switzerland*

[2]*National Cooperative for the Disposal of Radioactive Waste (NAGRA), Hardstrasse 73, 5430 Wettingen, Switzerland*

[3]*Geomechanica Inc., 90 Adelaide Street West, Toronto, Ontario M5H 3V9, Canada*

[4]*French National Agency for Radioactive Waste Management (ANDRA), RD 960, 55290 Bure, France*

[5]*Nuclear Waste Management Organization, 22 St Clair Avenue East, Toronto, Ontario M4T 2S3, Canada*

[6]*Federal Institute for Geosciences and Natural Resources, Stilleweg 2, 30655 Hannover, Germany*

**Corresponding author (e-mail: andres.alcolea@tkconsult.ch)*

Abstract: The excavation damaged zone (EDZ) around the backfilled tunnels of a geological repository represents a possible release path for radionuclides, corrosion and degradation gases that needs to be adequately addressed by safety assessment (SA) modelling tools. The hydromechanical phenomena associated with the creation and temporal evolution of the EDZ are of high complexity, precluding detailed representations of the EDZ in conventional SA. Thus, simplified EDZ models mimicking the safety-relevant features of the EDZ are required. In this context, a heuristic modelling approach has been developed to represent the creation and evolution of the EDZ in an abstracted and simplified manner. The key features addressed are the stochastic character of the excavation-induced fracture network and the self-sealing processes associated with the re-saturation after backfilling of the tunnels. The approach has been applied to a range of generic repository settings to investigate the impact of repository depth and *in situ* conditions on the hydraulic significance of the EDZ after repository closure. The model has been benchmarked with a dataset from a self-sealing experiment at the Mont Terri underground rock laboratory (URL), demonstrating the ability of the approach to mimic the evolution of the hydraulic significance of the EDZ during the re-saturation phase.

At the Cluster Conference in Luxembourg (November 2003) dedicated to the 'Impact of the Excavation Disturbed or Damaged zone (EDZ) on the Performance of Radioactive Waste Geological Repositories', a general definition of the EDZ around underground excavations was agreed upon by the scientific community:

> The Excavation Damaged Zone (EDZ) is a zone with significant irreversible processes and significant changes in flow and transport properties. These changes, for example, can include one or more orders of magnitude increase in flow permeability. (Tsang *et al.* 2005)

In recent years, the EDZ has been a focus of continuous international research activities, covering the key processes, phenomena and features associated with the creation and evolution of the EDZ for a variety of host-rock formations, including crystalline rock, rock salt, soft clays and indurated clays (Alheid *et al.* 2007; Aranyossy *et al.* 2008). Soft clays and indurated clay formations were identified as a class of sedimentary rocks with a distinctive deformation behaviour, displaying transitional features between ductile yielding and brittle failure in response to the excavation process. In the context of radioactive waste disposal, special emphasis has

From: NORRIS, S., BRUNO, J., VAN GEET, M. & VERHOEF, E. (eds) *Radioactive Waste Confinement: Clays in Natural and Engineered Barriers*. Geological Society, London, Special Publications, **443**, http://doi.org/10.1144/SP443.8

been given to the favourable capacity of EDZ fractures in clay formations to self-sealing after closure of the backfilled repository structures (Bernier *et al.* 2007; Blümling *et al.* 2007; Bock *et al.* 2010).

The Opalinus Clay, an indurated clay formation in the Molasse Basin of northern Switzerland, has been identified as a candidate host rock for a geological repository for radioactive waste in Switzerland. The EDZ around excavated openings in the Opalinus Clay Formation is predominantly a zone of brittle failure, as confirmed by multiple pieces of evidence gained during construction of motorway and railway tunnels (e.g. Steiner *et al.* 2010). In the long term, the fractures forming the EDZ are expected to re-seal in response to the re-saturation process and the corresponding pore-pressure recovery.

Quantitative analyses in support of the assessment of long-term radiological safety of geological repositories are often based on simplified representations of the EDZ, assuming a configuration of concentric shells (single shell or double shell, respectively) with enhanced hydraulic conductivity. The radius of the shell representing the EDZ typically depends on the tunnel radius and on the orientation of the tunnel axis with respect to the principal horizontal stress direction (e.g. NAGRA 2002). Several numerical EDZ abstraction approaches have been proposed in recent years, from complex EDZ fracture networks to simplified representations with equivalent flow and transport characteristics. Lanyon & Senger (2011) developed a sequential modelling approach for indurated clay formations, based on a stochastic representation of the EDZ in terms of discrete fracture network (DFN) models. The underlying hydraulic DFN models with stochastic distributions of fracture frequency, orientation and transmissivity were converted into equivalent-porous-medium (EPM) models with stochastic permeability distribution using the approach suggested by Jackson *et al.* (2000). Combined water and gas flow along stochastic realizations of the EDZ was simulated with the EPM models. Eventually, effective properties suitable for performance assessment were derived by inverse modelling of the results of stochastic modelling, with a simple single-shell representation of the EDZ. Hawkins *et al.* (2011) presented a similar approach with applications to the Meuse/Haute Marne underground rock laboratory (URL) in the Callovo-Oxfordian Formation in the NE Paris Basin.

The aforementioned approaches for the simplification of the EDZ draw on stochastic representations of the EDZ fracture network derived from structural mapping in tunnels. This work presents a novel heuristic modelling approach based on EDZ fracture networks derived with a fracture-mechanics-based numerical model. Thus, the impact of stress conditions, rock strength and tunnel geometry on fracture patterns can be assessed in a systematic manner using parametric sensitivity analyses. The approach is able to mimic the safety-relevant features of the EDZ in an abstracted and simplified manner. This paper is organized as follows. First, the conceptual framework for the hydraulic significance of the EDZ is outlined. Second, the methodology is presented in detail. Third, the results of a sensitivity analysis of the hydraulic significance of the EDZ to various repository settings are explored. Finally, the application and benchmarking of the abstraction approach to the HG-A experiment ('Gas path through host rock and along seal sections') is presented.

Conceptual framework

Empirical and experimental evidence

When a geological repository is constructed in an indurated clay formation, the host rock around the newly created openings is expected to respond in a brittle manner. Part of the irreversible deformation already occurs as pre-deformation ahead of the tunnel face (Martin 1997; Yong 2008), whereas the development of the system of excavation-induced fractures continues during the excavation process and even after completion of the permanent tunnel support system (Blümling *et al.* 2007). The shape and extension of the EDZ around the openings are controlled by many factors, including the general geological setting (e.g. rock mass strength, stress and pore-pressure distribution, sedimentary and tectonic features, and *in situ* stress field), engineering design (e.g. configuration of the underground structures, excavation technique and support system/lining) and the impacts related to the operational phase (e.g. ventilation and waste emplacement). Rock deformation is complicated by clay-specific hydromechanical couplings, giving rise to long-lasting time-dependent processes in the EDZ even after closure of the backfilled repository structures. A typical inventory of discrete EDZ features consists of extensional fractures (Fig. 1a), caused directly by the short-term excavation-induced unloading (undrained elasto-plastic response), spalling and buckling of the bedding planes (Fig. 1b, c), interactions with the existing tectonic features (Fig. 1b), and bounding shear bands. These features delimit the EDZ and the intact rock zones (Blümling *et al.* 2007). Further EDZ features can be attributed to the operational phase, such as desiccation cracks in response to tunnel ventilation and swelling-induced disaggregation of the rock matrix, when subjected to water-based fluids (e.g. cement water during construction of the invert).

The characterization of structural and hydromechanical features and processes of the EDZ has been

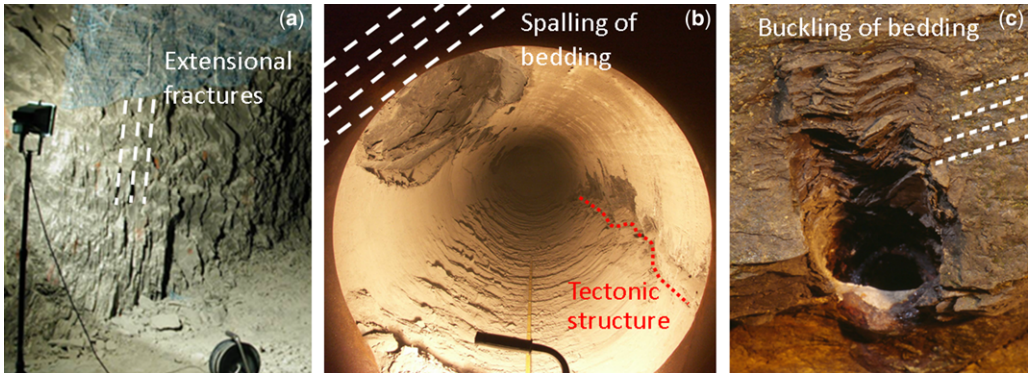

Fig. 1. Excavation-induced brittle features in Opalinus Clay (Mont Terri URL): (**a**) extensional fractures created during the excavation of Gallery 98 (NAGRA 2002); (**b**) bedding-related spalling processes in the crown of the HG-A microtunnel and the interaction of stress-controlled failure at the lower-right side wall with a tectonic structure (Marschall *et al.* 2006); and (**c**) buckling of the bedding planes around a small borehole (Blümling *et al.* 2007).

a key research topic in the scientific programme of the Mont Terri URL in Switzerland. Early work by Martin & Lanyon (2003) and Corkum & Martin (2007) focused on the EDZ around tunnel sections normal to bedding strike, drawing on previous work from Bossart *et al.* (2002). More recently, emphasis was given to excavations parallel to bedding strike because these configurations are more relevant for a future deep repository (Marschall *et al.* 2006; Lanyon *et al.* 2014; Lisjak *et al.* 2015). The impact of pre-existing tectonic features on the development of the EDZ was highlighted by Yong (2008) and Nussbaum *et al.* (2011). Yong (2008) reported a comparison of fracture density in boreholes around tunnels and niches at Mont Terri, examining data from over 100 boreholes (Fig. 2a). All structures, other than those clearly related to tectonic features or drill core handing, were counted over 0.5 m intervals. Almost 75% of the boreholes were drilled into the sidewalls and data were normalized per borehole to reduce the bias. Fracture count in the first 0.5 m can be as high as 10 (with a mean spacing 5 cm) around some excavations, but typically reduces to less than two at 3 m from the tunnel wall.

At the Mont Terri URL, small-scale *in situ* permeability measurements in the EDZ were carried out in boreholes equipped with multi-packer systems orientated radial to the drift, isolating measurement intervals of 10–50 cm at various distances from the wall. Hydraulic pulse and constant head tests were carried out in the saturated part of the EDZ, whereas simple pneumatic tests were undertaken in the unsaturated rock in the immediate vicinity of the tunnel surface to investigate the local effective permeability (Bossart & Thury 2008). Figure 2b shows that permeability increases by several orders of magnitude (up to six or seven) within 20–40 cm from the tunnel. This zone coincides with that exhibiting high fracture density.

Ferrari *et al.* (2013) and Romero & Gómez (2013) performed permeability tests in oedometric cells and triaxial cells on core samples from Mont Terri and from other locations in northern Switzerland to investigate the stress dependence of permeability and porosity of intact Opalinus Clay. A consistent trend in porosity and permeability reduction with increasing effective stress was observed, although each sample showed the influence of preconsolidation and mineralogy. Hydraulic conductivity was typically below 10^{-13} m s^{-1} for effective stresses greater than 20 MPa and reduced further to around 10^{-14} at 100 MPa (Fig. 3a). Clay content, porosity and specific surface data obtained from the laboratory analysis of Opalinus Clay samples were used to infer matrix hydraulic conductivity based on the Kozeny–Carman relationship (Alcolea *et al.* 2014).

The dependence of fracture transmissivity on normal effective stress has been the issue of laboratory studies and *in situ* tests (Blümling *et al.* 2007). As part of the GS ('Gasfrac Self-Healing') experiment at Mont Terri, hydraulic tests were performed in a borehole before and after a hydrofrac experiment. Testing was conducted in a test interval containing a hydrofrac with a well-defined fracture geometry. Interval transmissivity increased by five or six orders of magnitude when the injection pressure exceeded the normal stress on the fracture plane (Fig. 3b). For low injection pressures, however, the interval transmissivity was close to that of the intact rock ($T \leq 10^{-12}$ m^2 s^{-1}). These findings can be explained by the dependence of fracture transmissivity (or hydraulic conductivity) on effective

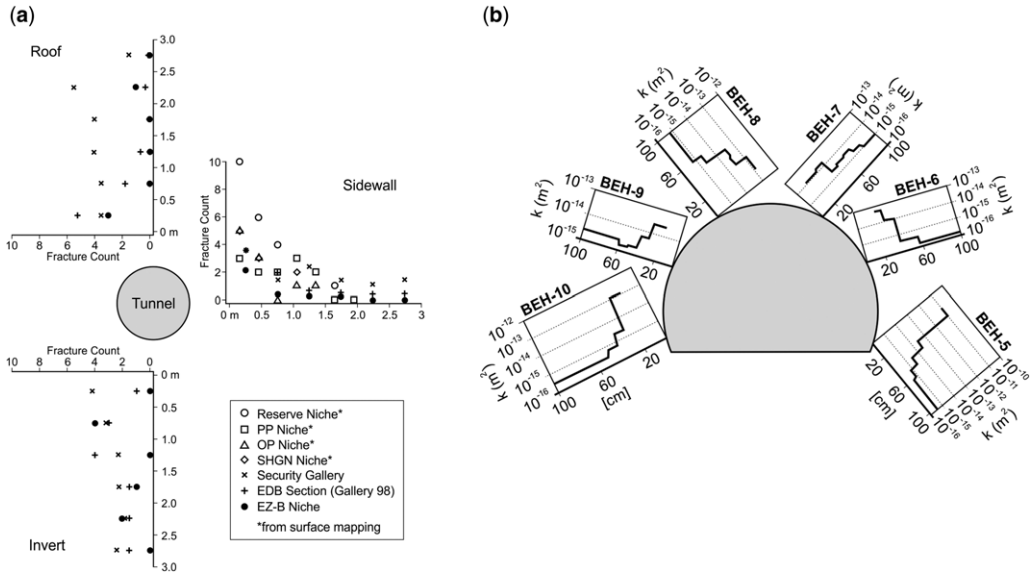

Fig. 2. Structural and hydraulic characterization of the EDZ features around excavations in the Mont Terri URL: (**a**) fracture counts in 0.5 m borehole intervals from around the EZ-B Niche and previous subparallel excavations (modified from Yong 2008); and (**b**) *in situ* permeability measurements conducted in Mont Terri experimental drift (from Bossart & Thury 2008).

normal stress, which follows a hyperbolic fracture closure law (see NAGRA 2004). An effective mechanical self-sealing of the artificial fracture was already observed at moderate effective normal stresses of the order of 1–2 MPa (Fig. 3b).

Further experimental evidence of the self-sealing capacity of excavation-induced fractures has been gained by *in situ* experiments at the Mont Terri URL, namely the SF experiment (Bernier *et al.* 2007) and the HG-A experiment (Lanyon *et al.* 2014). Notably, the long-term self-sealing tests in the HG-A microtunnel (Fig. 1b) served as a benchmark case for the modelling approach suggested in this work.

Conceptualization of fracture self-sealing

Drawing on the presented empirical and experimental evidence for the hydraulic significance of the EDZ during tunnel construction and its evolution during the operational phase and after backfilling of the underground structures, the functional

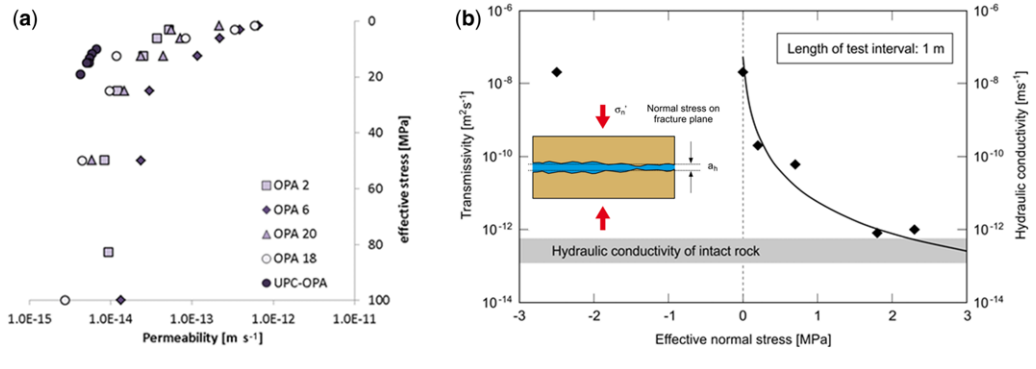

Fig. 3. Empirical relationships between stress and hydraulic properties of the host rock: (**a**) the stress–permeability relationship of the intact rock matrix; and (**b**) hyperbolic transmissivity–stress relationship between fracture transmissivity and normal effective stress (results of the GS experiment, from NAGRA 2004).

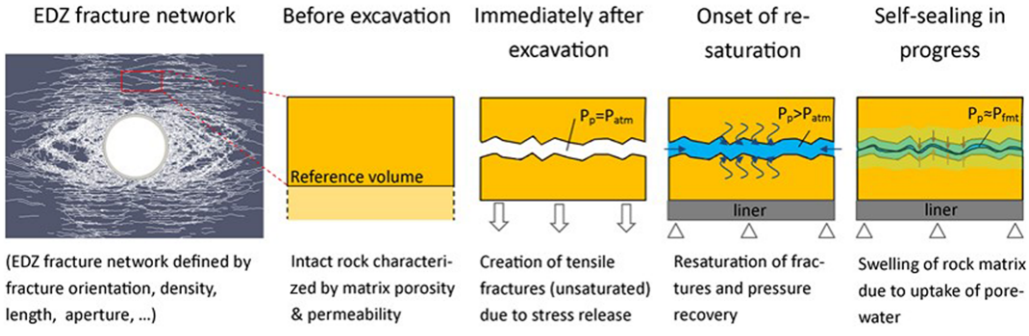

Fig. 4. Schematic sketch of the conceptual framework for EDZ fracture closure in Opalinus Clay, covering the key phenomena and features from the early post-excavation phase until static formation pressure recovery. In the insets, P_p denotes pore pressure, P_{atm} denotes atmospheric pressure and P_{fmt} denotes formation pressure.

requirements associated with a quantitative EDZ closure model can be formulated as follows (Fig. 4):

- The creation of the EDZ is a brittle process (i.e. the increase of the void volume in the damaged rock zone around the excavation is solely attributed to fracture opening, whereas the porosity of non-fractured rock remains essentially unchanged during the early times after excavation).
- Initially, the newly created EDZ fractures are unsaturated and exposed to atmospheric pressure, whereas the non-fractured rock remains saturated and exhibits high matrix suction as a consequence of the high gas entry pressure of the Opalinus Clay (Ferrari *et al.* 2014). The initial transmissivity of the unsaturated EDZ fractures is controlled by the fracture aperture and can be very high. The matrix conductivity remains essentially unchanged (i.e. it is the same as the conductivity of the intact rock).
- With time, the matric suction in the rock matrix decreases due to the uptake of porewater from outer rock zones, and the fractures start to resaturate.
- Porewater uptake of the non-fractured rock zones is associated with swelling and, consequently, with an increase in matrix porosity. The porosity increase of the rock matrix occurs at the expense of fracture aperture (i.e. the fractures start to close and fracture transmissivity reduces drastically, whereas the hydraulic conductivity of the non-fractured matrix zones increases slightly as a consequence of the porosity increase).
- This increase in matrix porosity and hydraulic conductivity is associated with the decrease in the fracture aperture and transmissivity, and progresses until the equilibrium of effective stresses is reached. This is essentially the case, when pore pressure reaches the static formation pressure.

A numerical approach for modelling the hydraulic significance of the EDZ is developed in the next section with the following goals: (i) to cope with a wide range of geological, hydrogeological and geomechanical conditions relevant to the candidate siting regions for a geological repository in northern Switzerland; (ii) to cover the relevant hydraulic and geomechanical phenomena and processes associated with the creation of the EDZ during construction, and its evolution during operational times and after backfilling of the underground structures; and (iii) to consistently capture the experimental evidence of the EDZ self-sealing, which has been gained as part of *in situ* experiments in URLs (e.g. the HG-A experiment at Mont Terri).

The methodology presented herein consists of three sequential main steps (Fig. 5). First, a hybrid finite-discrete element method (FDEM) (Geomechanica 2013, 2014; Lisjak *et al.* 2015, 2016) is used to simulate the geometry and geomechanical conditions of the DFNs forming the EDZ (Fig. 5a). The FDEM simulations are purely mechanical and mimic the excavation and emplacement processes. Secondly, the geometrical properties simulated by the FDEM are mapped onto a finite element mesh (Fig. 5b), which allows the fluid motion equations in the excavation near field to be solved. A salient feature of the suggested methodology is that hydraulic parameters of both fracture and matrix evolve with time as a response to re-saturation of the tunnel surroundings. Thirdly, an abstraction of the complex model is made based on the late-time behaviour (after full re-saturation) of the system (Fig. 5c). The main outputs of the model are the spatio-temporal distributions of hydraulic parameters and the corresponding specific fluxes towards the tunnel, with special emphasis on the late-time behaviour. Finally, the abstraction of the EDZ is implemented by defining a piecewise homogeneous 'shell-like' model with hydraulic behaviour identical to that of the complex model.

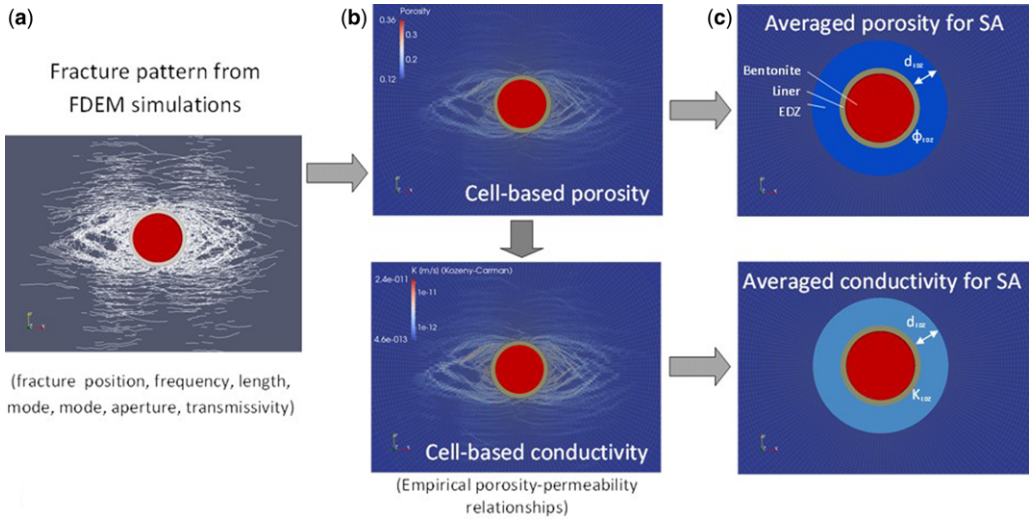

Fig. 5. Concept of the EDZ abstraction process for safety assessment (SA) applicable to a circular tunnel: (**a**) representative fracture patterns are simulated for relevant repository configurations with a discrete element model (FDEM); (**b**) the discrete fracture patterns are converted into heterogeneous porosity and conductivity distributions; and (**c**) in a final abstraction process, the heterogeneous porosity–conductivity distributions are converted in a shell defined by a radius and homogeneous porosity–conductivity.

The present study focuses on the temporal evolution of hydraulic parameters of the EDZ around the tunnel. For illustration purposes, the methodology is applied to the HG-A experiment at the Mont Terri URL.

Modelling approach

Following Lanyon & Senger (2011), an EPM representing a cross-section orthogonal to the axis of the underground structure is used to model the re-saturation of the EDZ. Re-saturation leads to the self-sealing of the EDZ by virtue of mechanical closure of fractures and swelling of the clay-rich minerals of the rock matrix. The modelling approach consists of three basic tools (Fig. 6): (1) mapping of the FDEM geometrical properties; (2) the re-saturation model, which calculates the pressure state of the system at a certain re-saturation stage and updates the FDEM parameters accordingly; and (3) EDZ abstraction. These tools are described in detail below and are applied to an illustrative example.

Mapping of the FDEM to an equivalent-continuum model

The fluid flow caused by the re-saturation of the EDZ is predominantly radial towards the tunnel owing to the shape of the EDZ and of the underground structure. Therefore, a radial finite element mesh is used, thus helping to alleviate the numerical artefacts caused by structured meshes while solving radial flow and reducing the computational time. A zonation of hydraulic parameters is also adopted to assign different properties to different materials (Table 1). The mesh is finer at the zone encompassing the EDZ. Cell size increases according to a geometric progression. Hydraulic properties at the cells are calculated from geometrical properties of the FDEM. To this end, the properties of fractures intersecting each cell (if any) are upscaled.

Cell porosity is calculated as:

$$\phi = \frac{V_p}{V_{tot}} = \frac{V_{p,f}(t) + (1 - (V_{p,f}(t)/V_{tot}))V_{p,m}(t)}{V_{tot}} = \phi_f(t)(1 - \phi_m(t)) + \phi_m(t) \quad (1)$$

where ϕ [−] is total porosity, V_p and V_{tot} [L^3] are the void volume and total volume of the cell, respectively, and t [T] is time. The numerical model is based on a unit length in the axial direction of the tunnel. Therefore, cell volumes are equivalent to cell areas. Subscripts 'f' and 'm' refer to fracture and matrix, respectively. Constant deterministic values of matrix porosity for the different materials defining the model zonation are summarized in Table 1.

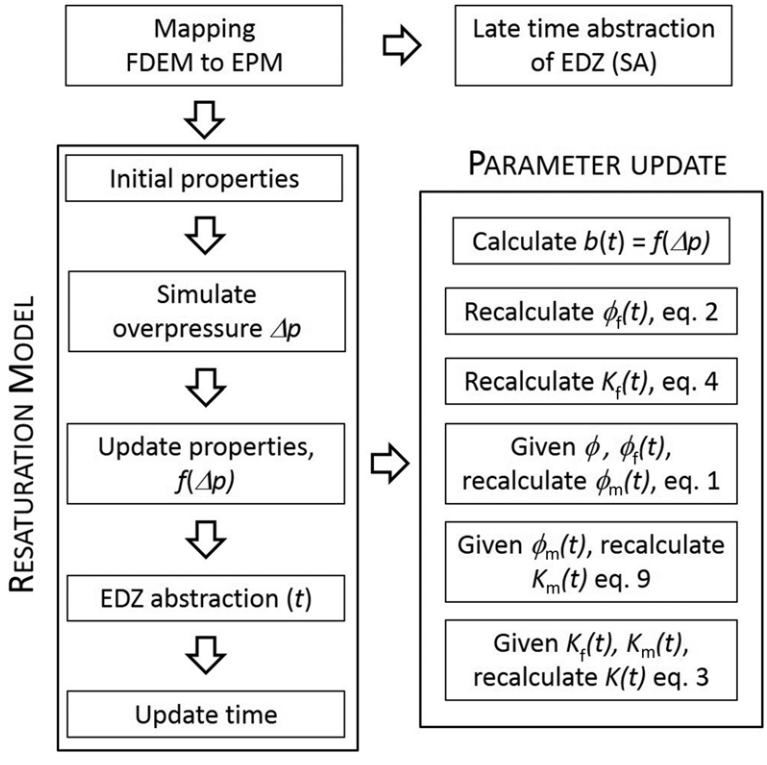

Fig. 6. Suggested modelling approach. The starting point is a mechanical simulation of the EDZ after excavation. Geometrical properties of the fractures delineating the EDZ are mapped to a continuum model. After mapping, and assuming that all fractures are closed (i.e. attributed with a residual aperture/irreducible transmissivity), the late-time behaviour of the EDZ ($t > 20\,000$ years) is analysed and an abstraction consisting of a piecewise homogeneous model is proposed. Such abstraction is amenable to SA analysis. In addition, the temporal evolution of the EDZ during re-saturation can also be addressed by the continuum model. A decoupled hydromechanical model is posed that updates fracture aperture at each time step as a function of overpressure (i.e. above atmospheric pressure). Hydraulic properties of the EDZ vary in time in response to re-saturation. The EDZ abstraction can therefore be made at intermediate times of re-saturation. In the insets, t denotes time, b is aperture, K is the hydraulic conductivity and ϕ is porosity. Subscripts f and m denote fracture and matrix, respectively.

Fracture porosity of a given cell is calculated as an average of the geometrical parameters defining the fractures intersecting the cell:

$$\phi^{j}_{\mathrm{f}}(t) = \frac{\sum_i b_i(t) L^j_i}{V_j} \qquad (2)$$

where b_i [L] and L^j_i [L] are the aperture and trace length of fracture i intersecting cell j. V_j is the cell volume (area).

Hydraulic conductivity of a cell K [LT^{-1}] is calculated as:

$$K(t) = K_{\mathrm{m}}(t) + K_{\mathrm{f}}(t) \qquad (3)$$

where K_{m} [LT^{-1}] denotes hydraulic conductivity of the matrix (Table 1) and K_{f} [LT^{-1}] is fracture conductivity of cells intersected by fractures (0 otherwise). K_{f} is calculated from fracture trace length and transmissivity, calculated from fracture aperture using a cubic law approximation:

$$K^j_{\mathrm{f}} = \frac{\sum_i T_i(t) L^j_i}{V_j}; \quad T_i = \frac{\rho g b(t)^3_i}{12\mu} \qquad (4)$$

where T_i [$\mathrm{L}^2\mathrm{T}^{-1}$] is the transmissivity of fracture i intersecting cell j, g is gravity [LT^{-2}], and ρ [ML^{-3}] and μ [$\mathrm{ML}^{-1}\mathrm{T}^{-1}$] are the fluid density and dynamic viscosity, respectively.

Within the modelled cross-section, the flow occurs mainly in the fracture plane (i.e. along its longest edge). Thus, anisotropic hydraulic conductivities are calculated from the maximum

Table 1. *Model zonation and deterministic values of hydraulic properties*

Zone	Approximate radial extent (m)	Porosity	In-plane conductivity	
			K_{xx} (m s^{-1})	K_{zz} (m s^{-1})
Canister	0–0.5	NA	NA	NA
Bentonite (buffer zone)	0–1.25	0.35	10^{-13}	10^{-13}
Steel liner	1.25–1.5	0.20	10^{-10}	10^{-10}
EDZ	Variable	Variable	Variable	Variable
Intact Opalinus Clay (far field)	$R_{model} = 120$	0.12	10^{-13}	2×10^{-14}

The canister, emplaced at the centre of the model, is not simulated. Instead, a no-flow boundary condition is set there. R_{model} denotes the radius of the outer boundary of the model.

conductivity by standard projection:

$$K_{f,xx}(t) = K_f(t)\cos\theta$$
$$K_{f,zz}(t) = K_f(t)\sin\theta \quad (5)$$

where θ is the inclination of the fracture (measured counter-clockwise from the positive x-axis). x and z are local Cartesian axes in the plane of the cross-section. The positive y-axis runs along the tunnel towards its end.

Hydraulic conductivities in the x- and z-directions are then calculated at each cell:

$$K_{xx}(t) = K_{f,xx}(t) + K_{m,xx}(t)$$
$$K_{zz}(t) = K_{f,zz}(t) + K_{m,zz}(t)\ . \quad (6)$$

Finally, cell conductivity, K_{yy}, orthogonal to the cross-section (i.e. parallel to the axis of the opening) is calculated as:

$$K_{yy}(t) = \sqrt{K_{xx}(t)\ K_{zz}(t)}. \quad (7)$$

In equation (7), it is assumed that the cell size is sufficiently small and that the anisotropy of hydraulic conductivity is not significant. Note also that equations (1) and (3) involve time-dependent hydraulic parameters. The way in which these parameters vary with time is described in the next subsection.

FDEM parameters at a certain re-saturation stage

The re-saturation of the system has two implications. On the one hand, an increase in pressure inside the fractures (from atmospheric to hydrostatic conditions) causes a reduction in effective normal stresses. This reduction is assumed to be insufficient to either stimulate existing fractures (i.e. fracture trace length is constant) or to generate new fractures. Yet, the reduction of effective stresses ($\sigma > 0$ means compression) leads to mechanical closure of fractures. Fracture closure leads to a reduction in fracture porosity and hydraulic conductivity, according to equations (2) and (4). On the other hand, the high percentage of clay minerals causes the matrix to swell at low-pressure variations (<2 MPa). Swelling causes both matrix porosity and matrix hydraulic conductivity to increase with time.

Based on previous analyses of the results of the GS experiment (Fig. 3b) (see also NAGRA 2004), fracture closure is accommodated in the model through a function relating fracture aperture and overpressure, Δp [ML^{-1}T^{-2}] (i.e. pressure above atmospheric):

$$b(t) = b_0\left(1 - \frac{1}{(b_0 K_{n0}/\Delta p(t))^{1-\alpha} + 1}\right); \quad \alpha < 1 \quad (8)$$

where b_0 is the initial fracture aperture (here, before the re-saturation starts, immediately after excavation and emplacement) and K_{n0} is the fracture normal stiffness (ML^{-2}T^{-2}: *c.* 920 MPa m^{-1}) (Yong *et al.* 2010). The exponent α controls the velocity of fracture closure and is referred to as the closure rate. Note that at early times ($\Delta p \rightarrow 0$), the aperture tends to the initial one, in the absence of pressure perturbations. Low α values lead to smaller apertures for a given value of overpressure (alternatively, for a given value of re-saturation time). Correspondingly, the time required for a full re-saturation of the system is smaller for small α values. α is estimated by assuming that, after full re-saturation, all fractures are closed and attributed with a residual aperture of $b_r = 8.9 \times 10^{-8}$ m, corresponding to an irreducible transmissivity of $T_r = 5.7 \times 10^{-16}$ m^2 s^{-1}, according to the cubic law in equation (4). The residual aperture is selected in such a way that, after full re-saturation (i.e. after a differential pressure $\Delta p \rightarrow 7.8$ MPa, from atmospheric to hydrostatic conditions), the fracture

hydraulic conductivity of the most conductive cell is small and equivalent to the matrix conductivity of the intact Opalinus Clay. This low residual transmissivity is in agreement with the results of the GS experiment at Mont Terri (NAGRA 2004) (Fig. 3b). Plugging Δp, b_r and a mean initial aperture $b_0 = 6.7{\cdot}10^{-4}$ m in equation (8) yields a α value of approximately -3.4.

Matrix porosity, $\phi_m(t)$, is calculated from $\phi_f(t)$ by assuming that the total porosity, ϕ, is constant during the re-saturation process (equation 1). This assumption can be justified by the fact that fracture porosity diminishes with time owing to mechanical closure caused by a reduction in effective stresses, whereas matrix porosity increases with time due to the swelling of the rock matrix. The rates of porosity reduction/increase of $\phi_f(t)$ and $\phi_m(t)$ are unknown and, therefore, it is assumed for simplicity that the two effects cancel each other out. Matrix porosity and hydraulic conductivity are related through the well-known Kozeny–Carman equation:

$$K_m(t) = \frac{\phi_m(t)^3}{(1-\phi_m(t))^2}\,\frac{\rho g}{\mu}\,\frac{d_{10}^2}{180} \qquad (9)$$

where d_{10} [L] is the particle size for which 10% of the soil is finer. d_{10} is calculated using the pair of porosity–hydraulic conductivity values of the intact Opalinus Clay given in Table 1, giving $d_{10} = 1.94 \times 10^{-8}$ m.

The re-saturation process is simulated using a numerical model with the zonation and deterministic parameters given in Table 1, and with the following boundary conditions: zero drawdown at the external boundary (i.e. the far field is not perturbed by the presence of the underground structure due to the low hydraulic conductivity of the intact Opalinus Clay); and zero flux at the inner zone representing the canister, which, for simplicity, is assumed to be impervious. The initial pressure condition is hydrostatic at cells not intersected by fractures. Otherwise, atmospheric pressure is imposed. At a given time, t, the overpressure distribution is calculated and fracture apertures are recalculated according to equation (8). Fracture transmissivities are then calculated according to the cubic law in equation (4). Then, fracture porosity and hydraulic conductivity are calculated according to equations (2) and (4).

Figures 7 and 8 display the temporal evolution of pressure and total hydraulic conductivity at selected times. Early stages of the re-saturation process are controlled by the high transmissivity of the many fractures defining the EDZ. This process is initially very fast, but very slow at mid and late times, when a certain degree of re-saturation has already been achieved. In fact, the buffer zone (backfilled with bentonite) and some fractures are initially unsaturated. A set of bi-phase scoping simulations was carried out to address the impact of the initial unsaturated state. It was observed that the saturation of the initially unsaturated pores takes less than 10 years. This time frame is negligible compared to the total time required for the full pressure recovery of the system (>20 000 years). Therefore, the initial unsaturated state was ignored in order to decrease the overall computational time. The time at which full re-saturation occurs is uncertain and largely depends on the closure rate, α. This issue is discussed later in this paper.

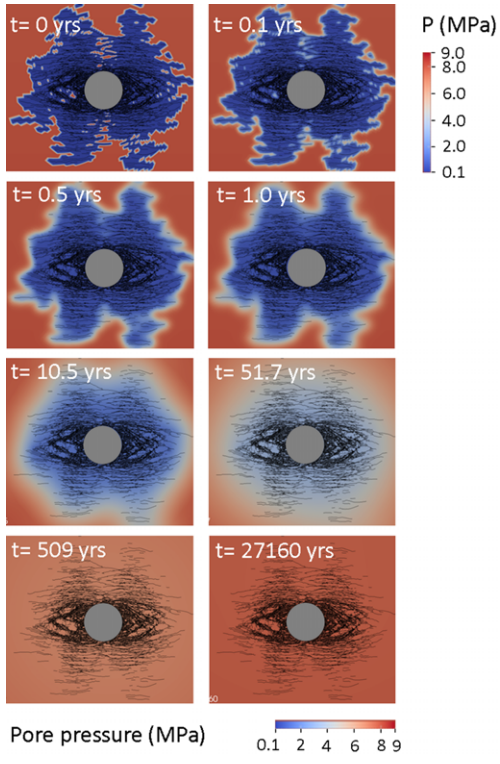

Fig. 7. Temporal evolution of pressure at selected time steps. Fractures defining the FDEM are superimposed (in black).

The temporal evolution of the system can be observed in Figure 9, which displays the number of closed fractures (i.e. those having residual aperture values) as a function of time. Most fractures are closed at early re-saturation times. This number steadily decreases with time and reaches a plateau after approximately 1000 years. The number of fractures defining the EDZ is >43 000. However, the number of closed fractures at the end of the simulation period is approximately 34 000. This means that full re-saturation of the EDZ was not achieved.

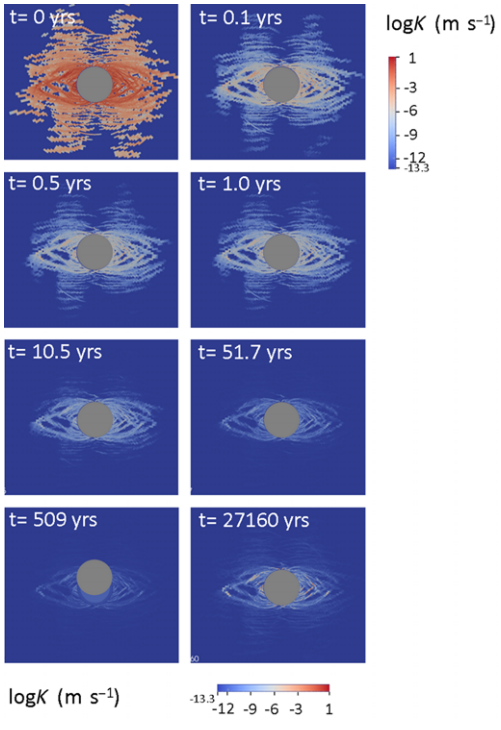

Fig. 8. Temporal evolution of axial hydraulic conductivity, K_{yy}, at selected time steps.

The fractures that remain open are clustered around the tunnel and are those with the largest initial aperture. The fast hydraulic response of the system is also observed in this plot.

Abstraction of the EDZ

This subsection describes the methodology for the abstraction of the EDZ. The abstraction consists of a simple piecewise homogeneous shell model that includes the liner, buffer zone, an equivalent EDZ and the intact Opalinus Clay (i.e. the far field). Homogeneous hydraulic properties are assigned to each zone. Hydraulic properties of the EDZ are averaged over its extent. Such abstraction is amenable to SA and frees the modeller from the burden of having to deal with complex, heterogeneous, EDZ models. Other geometrical conceptual models can be considered at this stage (e.g. elliptical zonation of the EDZ). The main advantage of the shell model proposed in this work, besides its simplicity, is that it allows the use of very simple analytical solutions or one-dimensional (1D) models for quick and simple calculations.

We consider the axial flow (i.e. parallel to the axis of the tunnel) through the modelled section, calculated as:

$$Q_y(r_i) = \sum_{j \in \text{shell } i} K_y^{i,j} A_{i,j} \tag{10}$$

where r_i [L] denotes the radius of a shell i, j is a counter of cells defining that shell, $A_{i,j}$ is the cell area and $K_y^{i,j}$ denotes the axial hydraulic conductivity (equation 7). Q_y (r_i) [L^3T^{-1}] is the axial flow rate under unit hydraulic head gradient between the extremes of the tunnel (i.e. the hydraulic conductance). To eliminate spurious mesh-related effects, Q_y is normalized by the area of the shell, thus becoming a specific flux, q_y [LT^{-1}]. Under unit hydraulic head gradient conditions, the specific

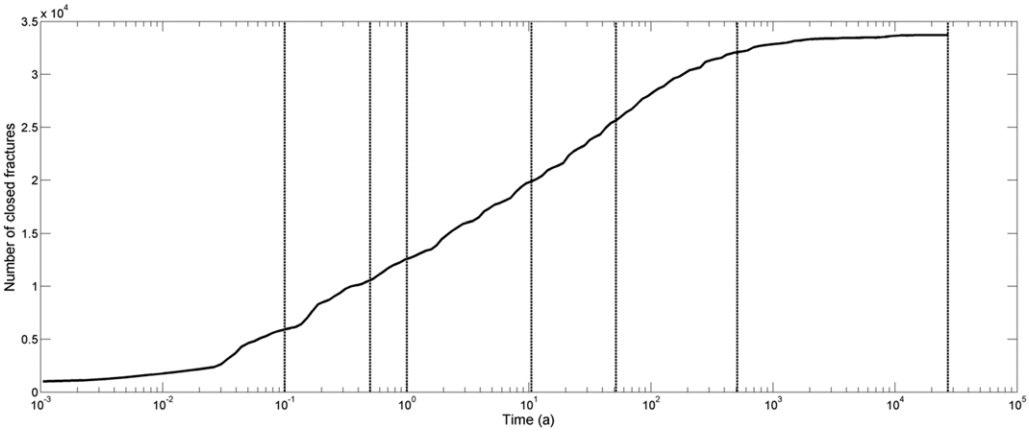

Fig. 9. Number of closed fractures v. time. The FDEM is made of 43 000 fractures. Vertical dashed lines depict the time steps in Figures 7 and 8.

flux at a certain shell is the average of the axial hydraulic conductivity.

Figure 10 depicts the temporal evolution of the equivalent EDZ hydraulic conductivity and the flow rate across the abstracted EDZ, Q_y. The equivalent hydraulic conductivity of the EDZ (or, equivalently, the total circulating flow rate) drops by approximately 11 orders of magnitude due to the mechanical closure of fractures and the swelling of the clay-rich materials of the rock matrix.

Notwithstanding the radial fluxes from/to the tunnel caused by regional (i.e. large-scale) porewater flow conditions in the host-rock formation, the axial fluxes and porosities at late times (i.e. after full re-saturation of the system, when all fractures are closed) are most relevant to SA (Bengtsson *et al.* 1991; Poller *et al.* 2014). Several observations can be made based on Figure 11:

- The specific flux, q_y, across fractures drops by almost 14 orders of magnitude after full re-saturation of the system (Fig. 11a) and by 13 orders of magnitude when the matrix is considered (Fig. 11b). Note that the total axial flux is already the residual one (*c.* 10^{-13} m s^{-1}) approximately 6 m far away from the centre of the opening, corresponding to the equivalent radius of the EDZ.
- At early times (Fig. 11c), fracture porosity decreases several orders of magnitude along a very small radial distance of approximately 6 m (i.e. the equivalent radius of the EDZ). In contrast, matrix porosity remains unchanged because swelling of the rock matrix has not yet taken place. At late times (Fig. 11d), fracture porosity is reduced by approximately four orders of magnitude due to mechanical closure. Instead, matrix porosity increases and coincides with total porosity as all fractures are closed. In fact, there is no distinction between the red and black lines in Figure 11d.

The late-time spatial distributions of effective porosity, $\phi(r)$, and hydraulic conductivity, $K(r)$, are the subject of further analysis, given its relevance to SA. First, averaged profiles $\langle\phi(r)\rangle$ and $\langle K(r)\rangle$ are obtained at each shell of cells defining the mesh of the EPM. The arithmetic mean is adopted for the porosity profiles, whereas the geometric mean is used to estimate the averaged conductivity profiles. Second, the average values of void volume $\langle V_p\rangle$ and total axial flux $\langle Q\rangle$ are calculated by integration:

$$\langle V_p\rangle = \int_{r_0}^{R_{model}} [\phi(r) - \phi_m]\, r\, dr$$
$$\langle Q\rangle = \int_{r_0}^{R_{model}} [K(r) - K_m]\, r\, dr \qquad (11)$$

where r_0 [L] and R_{model} [L] are the radius of the unlined tunnel and of the modelled section, respectively. Third, $\langle V_p\rangle$ and $\langle Q\rangle$ are used to define the homogenized properties of the abstracted EDZ in

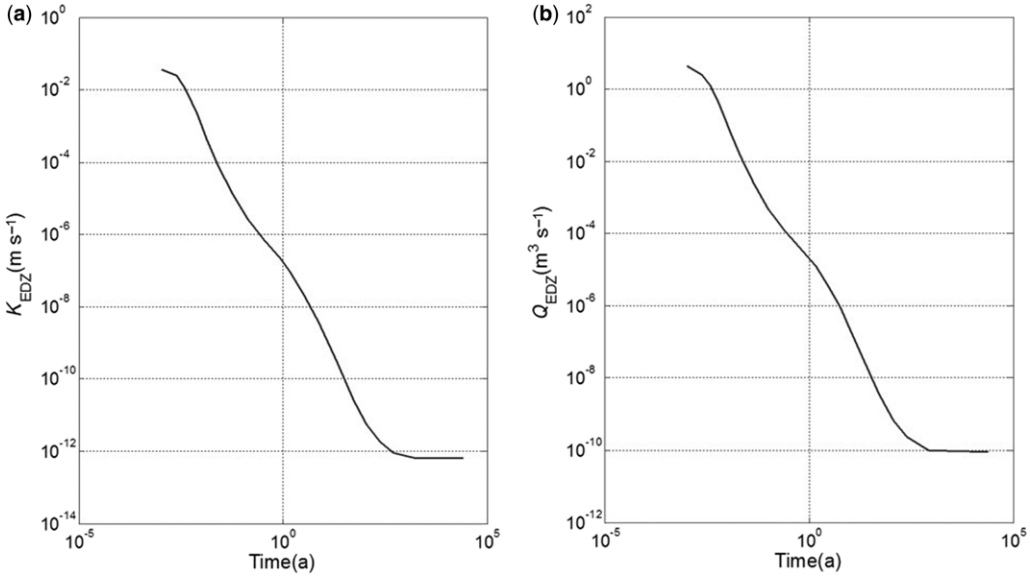

Fig. 10. Temporal evolution of (**a**) the equivalent axial hydraulic conductivity of the EDZ and (**b**) the axial flow rate.

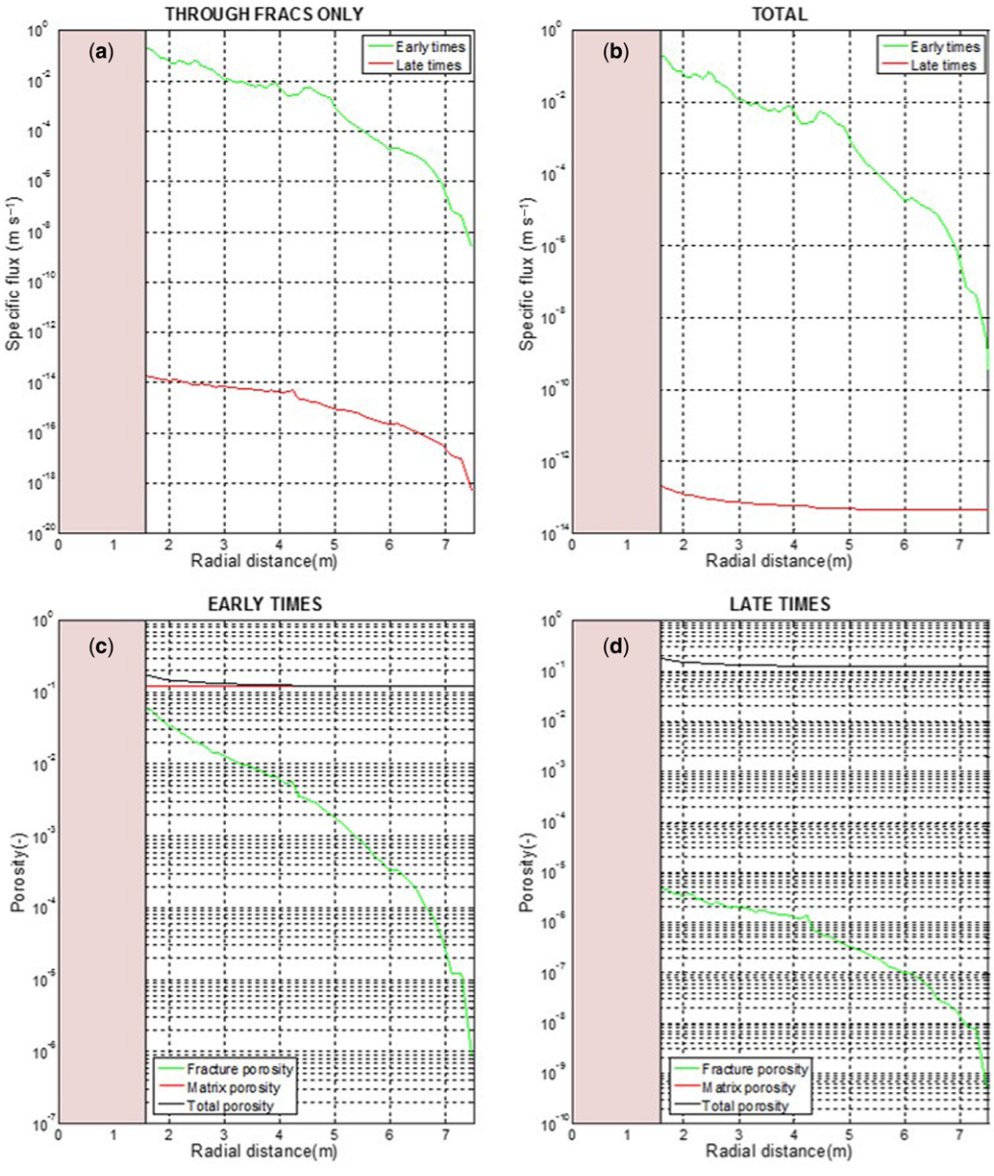

Fig. 11. Spatial distribution of: (**a**) the specific axial flux, q_y, through EDZ fractures only at early and late times; (**b**) the total specific axial flux at early and late times; (**c**) porosities at early times; and (**d**) porosities at late times ($t > 20\,000$ years).

terms of a relationship between the EDZ equivalent porosity, ϕ_{equiv}, hydraulic conductivity, K_{equiv}, and radius, r_{equiv}:

$$\phi_{\text{equiv}} = \phi_{\text{m}} + \frac{\langle V_{\text{p}} \rangle}{\pi(r_{\text{equiv}}^2 - r_0^2)}$$
$$K_{\text{equiv}} = K_{\text{m}} + \frac{\langle Q \rangle}{\pi(r_{\text{equiv}}^2 - r_0^2)}. \quad (12)$$

Sensitivity analysis

This section illustrates the sensitivity analysis of the EDZ significance to various repository settings, relevant to a deep geological repository in the proposed siting regions in northern Switzerland. Excavation-induced fracture patterns around the repository structures were simulated for repository depths of between 450 and 800 m below ground, horizontal to vertical stress ratios, $K_{\text{o}} = S_{\text{h}}/S_{\text{v}}$, of between

0.8 and 1.3, and rock mass strengths varying by a factor 5 around the reference values representative for the intact Opalinus Clay (Table 2) (Geomechanica 2013). Further simulations included stiff and soft tunnel support systems, and hypothetical repository configurations such as an intersecting fault system. A 3.0 m-diameter circular opening for the high-level waste SF-HLW emplacement tunnel (HAA hereinafter) is analysed in this study. Figure 12 displays simulated fracture patterns around the HAA cross-section for different repository depths (650 and 800 m below ground), different stress ratios ($K_o = 0.8$, 1.0 and 1.3), different rock strengths (low, reference, high) and different stiffnesses of the tunnel support (rigid, reference, soft). Notably, the fracture patterns exhibit marked differences in terms of size, shape and fracture intensity.

Alcolea *et al.* (2014) analysed the hydraulic behaviour of the EDZ at HAA cross-sections and also considered larger openings, such as shafts. The cross-sections of the HAA models were assumed perpendicular to the strike of flat-lying bedding planes (i.e. HAA models are vertical sections). The effect of the tectonic imprint on the EDZ response was investigated using five variants of the HAA model, in which three deterministic fractures dipping at 80° intersect the back and invert of the tunnel. These deterministic fractures have a thickness of 10 cm and are spaced at 0.5 m. Table 2 summarizes the main features of the simulations being analysed.

Figure 13a displays the radial distribution of fracture density, defined as the number of fractures within a given shell of mesh cells normalized by the area of the shell. The number of fractures close to the liner depends greatly on stress conditions and strength parameters under which the FDEM simulation was generated. However, a characteristic common to all FDEM simulations is that fracture density drops dramatically to almost negligible values at radial distances greater than about 4 m (radial distances are always measured with respect to the centre of the tunnel). The total extension of the EDZ (i.e. zero fracture density) is nearly the same for all FDEM models: approximately 8 m.

Table 2. *Summary of HAA model simulations*

Model	S_v (MPa)	S_h (MPa)	Strength properties	Elastic modulus of support (MPa)	Core-softening ratio γ	Number of EDZ fractures	Average aperture (mm)	Average initial transmissivity ($\log 10T$ ($m^2\ s^{-1}$))
Sensitivity to *in situ* stress conditions and core-softening ratio								
HAA-01	19.6	15.7	OPA × 2	32	0.01	43058	0.40	−4.28
HAA-02	19.6	19.6	OPA × 2	32	0.01	46366	0.40	−4.28
HAA-03	19.6	25.5	OPA × 2	32	0.01	55543	0.43	−4.19
HAA-04	19.6	15.7	OPA × 2	32	0.05	22419	0.30	−4.66
HAA-05	19.6	19.6	OPA × 2	32	0.05	25237	0.31	−4.62
HAA-06	19.6	25.5	OPA × 2	32	0.05	34891	0.36	−4.43
HAA-07	19.6	19.6	OPA × 2	32	0.008	50411	0.41	−4.26
HAA-08	15.9	20.7	OPA × 2	32	0.008	42331	0.41	−4.24
HAA-09	15.9	15.9	OPA × 2	32	0.003	36658	0.45	−4.11
Sensitivity to strength parameters								
HAA-10	15.9	20.7	OPA × 1.5	32	0.008	62413	0.37	−4.38
HAA-11	15.9	20.7	OPA × 3	32	0.008	18492	0.51	−3.96
HAA-12	15.9	20.7	OPA × 4	32	0.008	6697	0.68	−3.59
HAA-13	15.9	20.7	OPA × 5	32	0.008	3363	0.84	−3.32
Sensitivity to the presence of faults								
HAA-14	19.6	19.6	OPA × 2	32	0.01	56057	0.40	−4.28
HAA-15	19.6	19.6	OPA × 1.5	32	0.008	85324	0.38	−4.34
HAA-16	19.6	19.6	OPA × 3	32	0.008	25671	0.43	−4.20
HAA-17	19.6	19.6	OPA × 4	32	0.008	15037	0.45	−4.12
HAA-18	19.6	19.6	OPA × 5	32	0.008	9724	0.41	−4.26
Sensitivity to shotcrete stiffness								
HAA-19	15.9	20.7	OPA × 2	16	0.008	42376	0.41	−4.24
HAA-20	15.9	20.7	OPA × 2	3.2	0.008	43260	0.45	−4.13
HAA-21	15.9	20.7	OPA × 1.5	3.2	0.008	65376	0.40	−4.27
HAA-22	15.9	20.7	OPA × 3	3.2	0.008	19994	0.55	−3.86
HAA-23	15.9	20.7	OPA × 4	3.2	0.008	7378	0.71	−3.54
HAA-24	15.9	20.7	OPA × 5	3.2	0.008	3487	0.85	−3.30

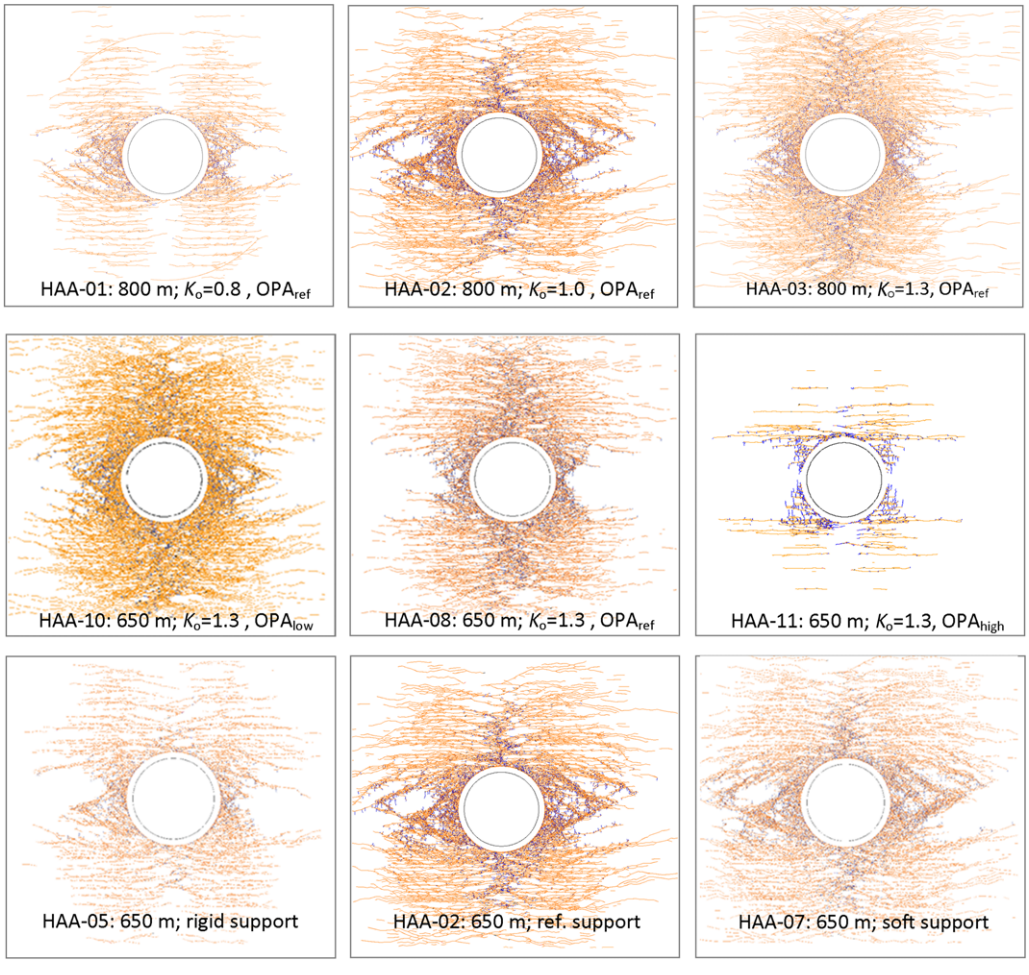

Fig. 12. EDZ fracture patterns around a circular SF-HLW emplacement tunnel ('HAA cross-section') simulated for various repository settings. The sensitivity cases comprise the variation of repository depth, the stress ratio $K_o = S_h/S_v$, the rock strength ($OPA_{low} = 0.5 \times$ reference strength, OPA_{ref}; $OPA_{low} = 3 \times OPA_{ref}$) and the stiffness of the tunnel support (stiff lining: core-softening ratio $\gamma = 0.003$; reference support: $\gamma = 0.01$; soft lining $\gamma = 0.05$). OPA denotes Opalinus Clay. Examples are taken from Geomechanica (2013).

Figure 13b displays the spatial distribution of matrix porosity after full re-saturation of the system. Swelling of the clay-rich materials forming the matrix increases matrix porosity from its initial value (0.12: Table 1) to values greater than 0.2. As observed, the sensitivity of the matrix porosity to different stress–strength conditions is large close to the liner. Yet, the overall sensitivity of matrix porosity is low at a radial distance of 2 m, even if fracture densities are still high.

Figure 13c, d depicts the fracture porosity at early and late times. Initial fracture porosities are high, up to 0.12, but drop drastically (more than five orders of magnitude) after full re-saturation of the system. The sensitivity of fracture porosity to stress–strength conditions and other factors defining the repository settings is also low. The same conclusion becomes apparent from Figure 13e, f, reporting on total specific fluxes. The very high initial transmissivity of the EDZ generates axial fluxes of up to 1 m s^{-1} (assuming unit gradient conditions). These drop substantially by more than 12 orders of magnitude after re-saturation of the system due to the mechanical closure of the fractures and the swelling of the clayey matrix.

Overall, the sensitivity of the hydraulic behaviour of the EDZ to repository depth, *in situ* stress conditions, rock mass strength and tunnel support system is low. The same conclusion can be drawn from Figure 14, which displays the homogenized

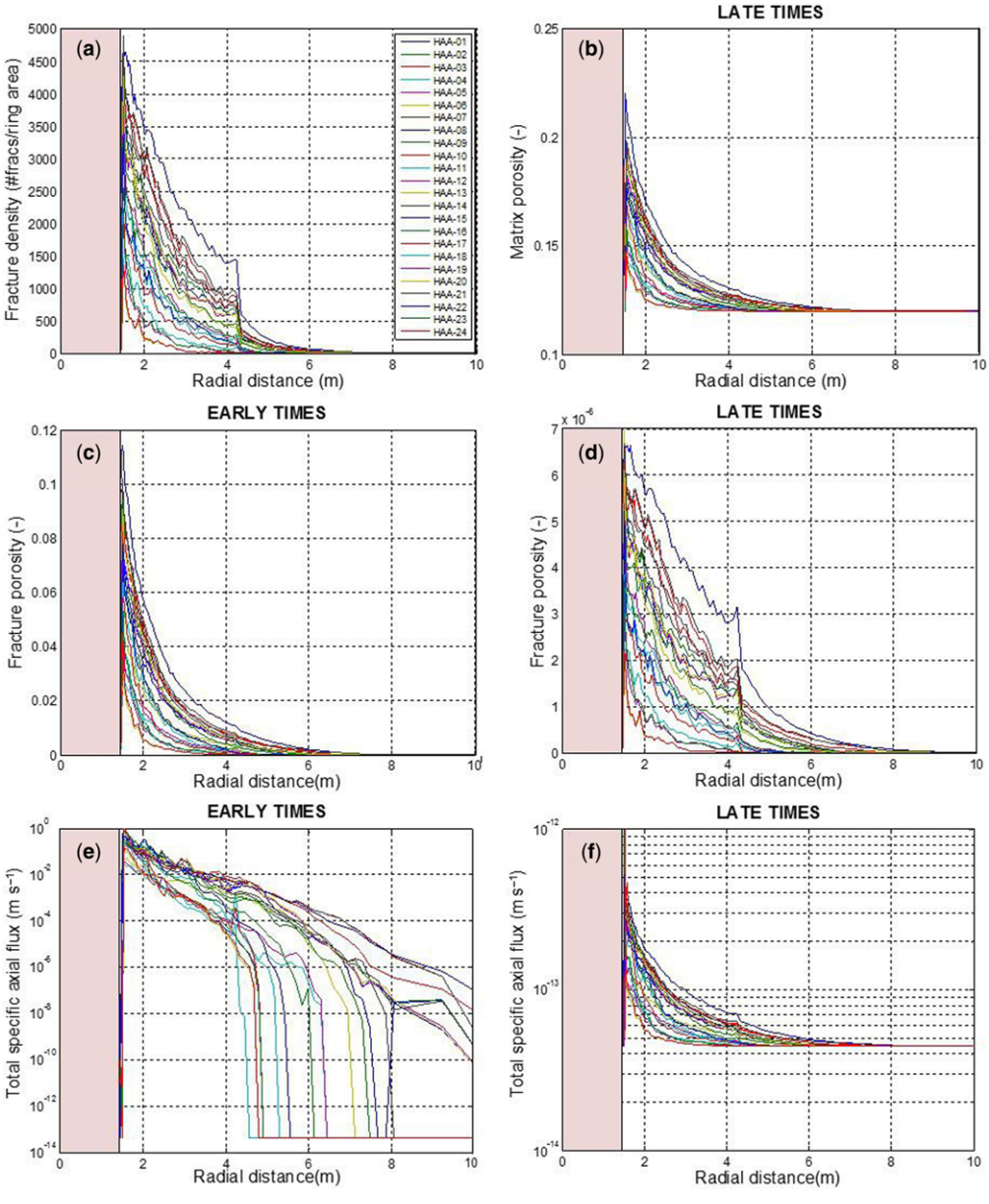

Fig. 13. Radial distribution of: (**a**) fracture density; (**b**) matrix porosity at late times, after full re-saturation of the system; (**c**) & (**d**) fracture porosity at early times after excavation and at late times, respectively; and (**e**) & (**f**) total specific axial fluxes at early and late times. The pink insets depict the buffer and liner zone.

equivalent properties of the EDZ. As observed, the radius of the EDZ is 5–6 m, regardless of repository settings. The choice of the EDZ radius and corresponding EDZ parameters (equation 12) is driven by the pragmatic considerations of the end-users' applications, such as probabilistic safety assessments. The similarity of results in terms of EDZ radius, despite the broad range of tested repository settings, is ascribed to the role of the extensile fractures, forming onion-like fracture patterns with significant fracture apertures in the immediate vicinity of the tunnel surface. The far-reaching shear fractures are characterized by smaller fracture apertures and emerge with a greater diversity

of fracture patterns in response to different *in situ* stress conditions or to the presence of tectonic imprint. This is reflected (1) in the geometry and fracture density of the EDZ and (2) in the hydraulic behaviour at early times, when all fractures are open. At late times, self-sealing of fractures takes place. This leads to a certain homogenization of the system because the contribution of the shear fractures to the total conductance of the EDZ reduces when compared to that of the extensile fractures in the immediate vicinity of the tunnel surface.

Application to the HG-A experiment

The suggested approach is benchmarked with a dataset from the HG-A experiment: an *in situ* self-sealing experiment at the Mont Terri URL in Switzerland. A 1 m-diameter, 13 m-long microtunnel was excavated during February 2005 using a steel auger from a niche in Gallery 04 of the URL. The microtunnel was excavated parallel to the strike of bedding planes dipping at about 50°. The first 6 m of the microtunnel was lined with a steel casing immediately after excavation in order to stabilize

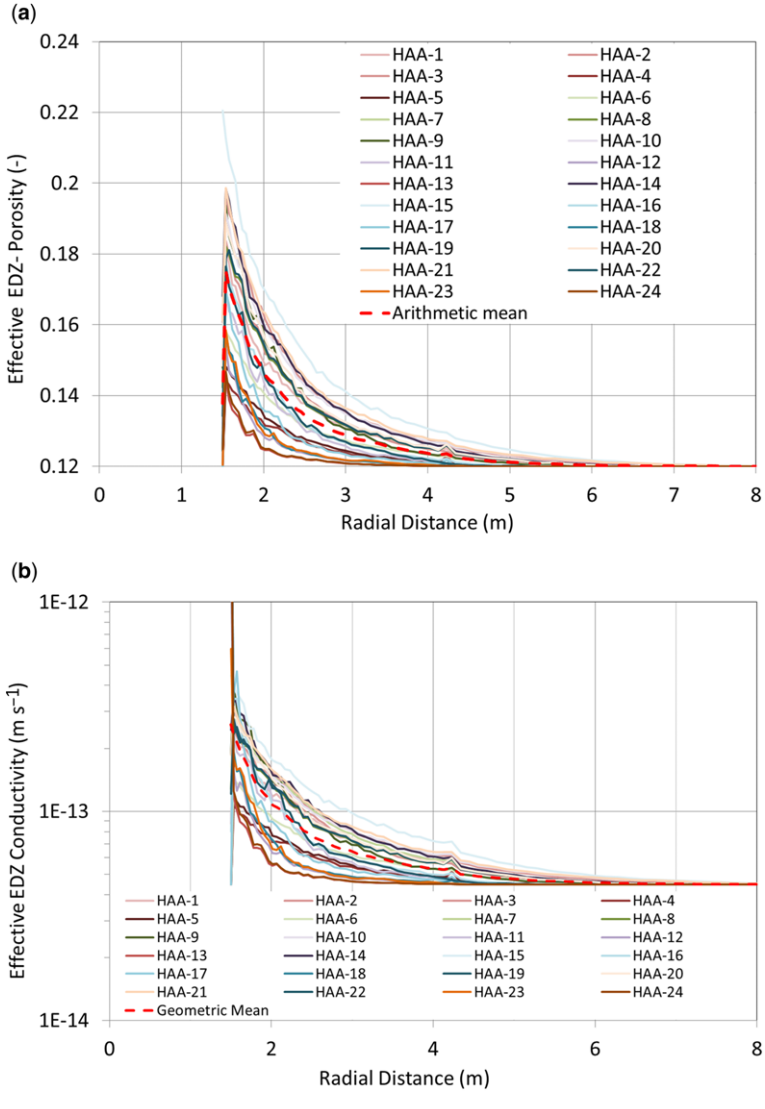

Fig. 14. Spatial distribution of equivalent porosity, ϕ_{equiv}, and equivalent hydraulic conductivity, K_{equiv}, for a variety of cases involving different repository depths, *in situ* stress conditions, rock mass strengths and tunnel support systems.

the opening. The gap behind the liner was then cement-grouted, but not sealed. A purpose-built hydraulic megapacker (diameter of 940 mm and sealing section length of 3000 mm) was installed in 2006. The sealing section was located at 6–9 m with a 1 m grouted zone containing the non-sealing part of the packer and a retaining wall from 9 to 10 m. The final 3 m of the microtunnel (from 10 to 13 m) formed the test section, which was instrumented and backfilled prior to megapacker emplacement (Fig. 15a) (see Lanyon *et al.* 2014 for further details).

Following emplacement of the megapacker, the 1 year-long saturation period was followed by extensive multi-rate injection testing over 2 years. Water was injected into the test section at the end of the micro-tunnel. During the multi-rate test, the injection rate was reduced from an initial

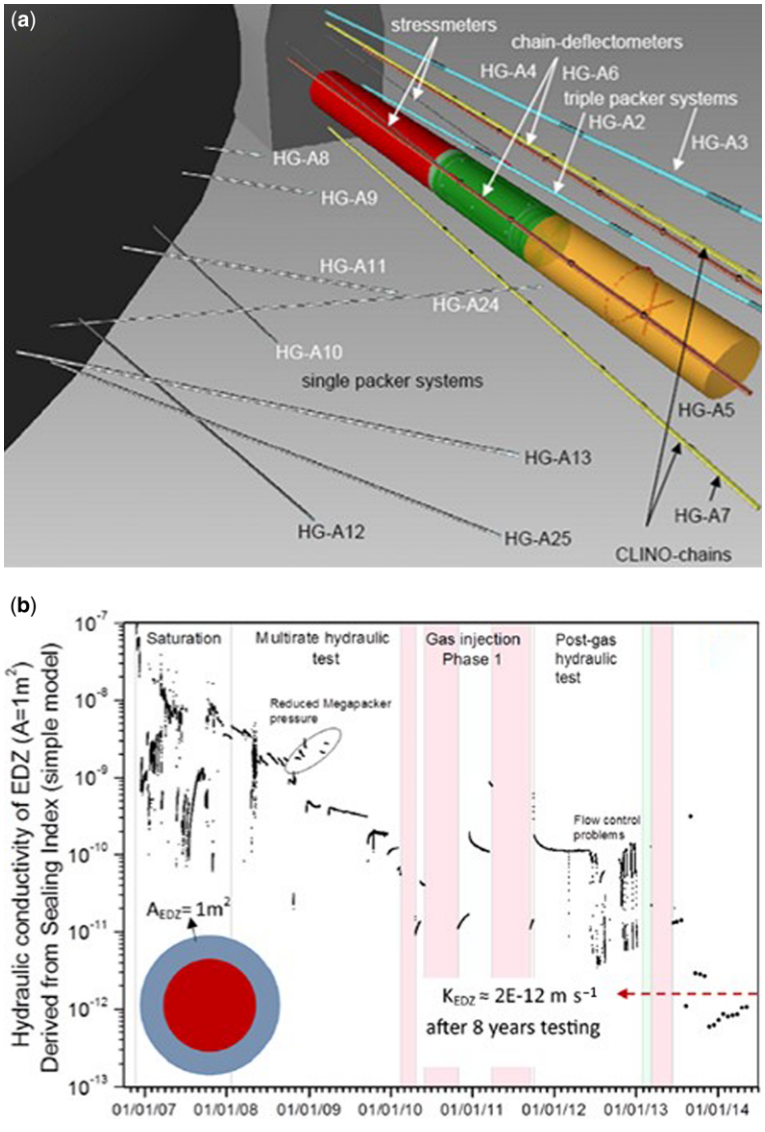

Fig. 15. (**a**) Layout and borehole instrumentation (colour coding: red, the steel liner: green, the seal section; orange, the backfilled test section). (**b**) Sealing index observed during the HG-A experiment. A significant reduction in the ability to inject water into the test section caused by the reduction of the EDZ conductive features is observed. At the end of the observation period, the effective hydraulic conductivity of an equivalent double-shell EDZ model with a cross-sectional area of 1 m^2 is around 2×10^{-12} m s^{-1}.

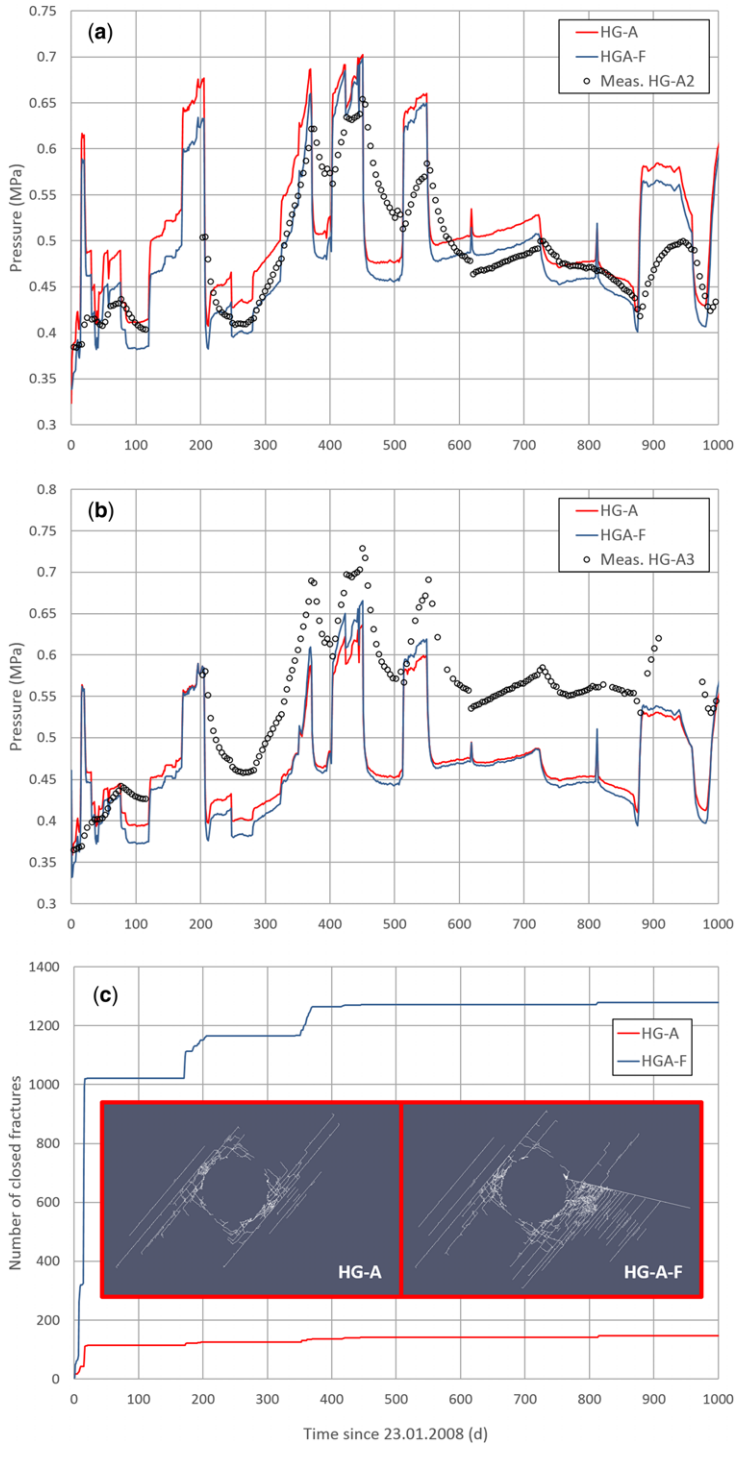

Fig. 16. (**a**) Pressure fits at observation borehole HG-A2 for simulations HG-A and HG-A-F; (**b**) pressure fits at observation borehole HG-A3; and (**c**) the number of closed fractures v. time. In the inset, the discrete fracture networks.

10 ml min^{-1} to less than 0.1 ml min^{-1} as the permeability of the EDZ dropped. The sealing index (SI), a simple measure of the hydraulic conductance of the EDZ, was calculated from the applied injection rate and the test section pressure, and is shown in Figure 15b. Assuming linear flow and a flow-path length of 3 m (seal section), the sealing index can be converted into an EDZ conductance (m^3 s^{-1}) by multiplying it by a factor of 5×10^{-7} (Lanyon *et al.* 2009, 2014).

The model applied for the benchmarking is slightly different to that presented in the previous section. In this case, we modelled a vertical cross-section at the seal section, and the canister and buffer zones were replaced by the megapacker. Available pressure measurements during the multi-rate injection test at the packered sections of observation boreholes HG-A2 and HG-A3 (Fig. 15a) were used in the calibration. Two parameters are calibrated by least-squares optimization: that is, the closure rate, α, and a dampening factor, β. The latter multiplies the prescribed pressure at the inner boundary condition (i.e. that caused by megapacker inflation/deflation) and mimics (a) a skin effect around the microtunnel and (b) the transfer of mechanical energy to fluid and solid phases in the vicinity of the megapacker external membrane. Two different FDEM models of the EDZ were considered: without and with tectonic fractures (Fig. 16b: models HG-A and HG-A-F, respectively). The model HG-A is initially not too transmissive compared to HG-A-F owing to its relatively low fracture density.

Figure 16a, b displays the pressure fits at observation boreholes HG-A2 and HG-A3 for both models. Note that the suggested modelling methodology is not aimed at obtaining good fits of available measurements for several reasons: (1) the model is 2D, whereas the reaction of the system to the re-saturation of the test section and to the inflation/deflation of the megapacker is clearly 3D (Lanyon *et al.* 2014); and (2) the hydraulic and mechanical responses are fully decoupled (actually, the elasto-plastic stress–strain equations are not solved). Instead, we seek a simple model, well suited to SA and capable of capturing the main physical processes caused by EDZ re-saturation. Such a simplistic model is shown to achieve relatively good fits of available measurements (see, for instance, the time period 300–400 days: Fig. 16a) and captures the main trends of the reaction to the forcing term measured at boreholes.

Best-fitting parameters are $\alpha = 1$ and $\beta = 1.05$ for HG-A, and $\alpha = 1$ and $\beta = 1.25$ for HG-A-F. The fact that a similar closure rate is attained by the two models (i.e. in the absence and presence of tectonic imprint) reveals that the calculated responses at observation points are not very sensitive to the geometry of the EDZ. However, the large difference between the best-fitting β factors shows the great sensitivity of the model to the hydraulic significance of the EDZ (Fig. 16c). In the absence of a tectonic imprint, fracture density is smaller and the forcing term, calibrated through the dampening factor β, is smaller. Instead, the higher EDZ transmissivities in the presence of tectonic imprint require a stronger forcing term to achieve the same goodness of fit.

Conclusions

The hydraulic significance of the EDZ around the backfilled underground structures of a geological repository has been identified as an important aspect in safety assessments (SAs). Indurated clay formations are characterized by brittle failure and complex coupled hydromechanical phenomena in response to the excavation process, precluding a detailed representation of the EDZ in conventional SA modelling tools. Instead, simplified models – still able to mimic the safety-relevant functional features of the EDZ – are required. This work presents a heuristic sequential modelling approach that is capable of representing adequately the key features and processes of the EDZ in indurated clays. First, brittle failure during the excavation process is simulated with a hybrid finite–discrete element code, providing realistic fracture patterns and fracture statistics that are in broad accordance with *in situ* observations. Secondly, EDZ self-sealing processes in response to pore-pressure recovery are modelled by the interplay of hydromechanical fracture closure mechanisms and swelling of the intact clay matrix. Thirdly, an abstraction towards a simplified shell-like representation of the EDZ is made. Such a simple model is hydraulically equivalent to the original discrete fracture network, but is amenable to SA.

A sensitivity analysis has been carried out to assess the hydraulic significance of the EDZ for various repository settings, relevant to a deep geological repository in the proposed siting regions in northern Switzerland. The sensitivity analysis included variations in repository depth, stress ratio, rock mass strength and design of the support system for a wide range of parameters. As a result, fracture patterns exhibiting marked differences in terms of size, shape and fracture density were obtained. The diversity of fracture patterns is reflected in the hydraulic simulations, which yield significantly different (several orders of magnitude) hydraulic conductances at early times of re-saturation. With time, the self-sealing of fractures takes place, causing fracture porosity and hydraulic conductivity to drop several orders of magnitude, and,

conversely, matrix porosity and hydraulic conductivity to increase. At late times (typically of the order of 20 000 years after repository closure), the EDZ is restricted to a radial zone with a radius of 5–6 m (equivalent to a thickness of less than two tunnel diameters) for all simulation cases. A significant enhancement of hydraulic conductivity is observed only in a zone with a thickness of less than half the tunnel diameter. There, the enhancement of effective hydraulic conductivity is less than one order of magnitude with respect to that of the intact rock matrix. Furthermore, the corresponding increase in porosity in this zone is less than 20% of the porosity of the intact rock matrix.

The methodology was then benchmarked with a dataset from an *in situ* self-sealing experiment at the Mont Terri URL, demonstrating the capacity of the modelling approach to mimic the evolution of hydraulic conductance of the EDZ around a backfilled tunnel section during the re-saturation phase. The fact that a simple model, which captures the main physical phenomena behind the long-term evolution of the EDZ, reproduces well the trends observed in available measurement records should be viewed as a hopeful step in the direction of abstracting simple models, amenable to safety assessment, from complex representations of the EDZ.

This work has been supported by the Swiss National Cooperative for the Disposal of Radioactive Waste (NAGRA) and the Mont Terri Consortium, representing the partners of the HG-A experiment ANDRA (France), BGR (Germany), NWMO (Canada), NAGRA and Swisstopo (Switzerland).

References

ALCOLEA, A., KUHLMANN, U., LANYON, G.W. & MARSCHALL, P. 2014. *Hydraulic Conductance of the EDZ Around Underground Structures of a Geological Repository for Radioactive Waste – A Sensitivity Study for the Candidate Host Rocks in the Proposed Siting Regions in Northern Switzerland*. NAGRA Arbeitsbericht NAB 13-94. NAGRA, Wettingen, Switzerland.

ALHEID, H.J., ARANYOSSY, J.F., BLÜMLING, P., HOTEIT, N. & VAN GEET, M. 2007. *EDZ Development and Evolution – State of the Art*. NF-PRO. Contract Number F16W-CT-2003-02389. European Commission, Luxembourg.

ARANYOSSY, J.F., MAYOR, J.C. *ET AL.* 2008. *EDZ Development and Evolution (RTDC 4) – Final Synthesis Report (D. 4.5.3)*. FP6-EURATOM/NF-PRO, F16W-CT-2003-02389. European Commission, Luxembourg.

BENGTSSON, A., GRUNDFELT, B., MARKSTROM, A. & RASMUSON, A. 1991. *Impact from the Disturbed Zone on Nuclide Migration – A Radioactive Waste Repository Study*. SKB Technical Report 91-11. SKB, Stockholm.

BERNIER, F., LI, X.L. *ET AL.* 2007. *Fractures and Self-healing within the Excavation Disturbed Zone in Clays (SELFRAC)*. Final Report, EURATOM, Fifth Framework Programme, Contract No. FIKW-CT2001-00182. European Commission, Luxembourg.

BLÜMLING, P., BERNIER, F., LEBON, P. & MARTIN, C.D. 2007. The excavation damaged zone in clay formations time-dependent behaviour and influence on performance assessment. *Physics and Chemistry of the Earth*, **32**, 588–599.

BOCK, H., DEHANDSCHUTTER, B., MARTIN, C.D., MAZUREK, M., DE HALLER, A., SKOCZYLAS, F. & DAVY, C. 2010. *Self-Sealing of Fractures in Argillaceous Formations in the Context of Geological Disposal of Radioactive Waste Review and Synthesis Report*. Radioactive Waste Management. OECD NEA 6184. NEA OECD, Paris.

BOSSART, P. & THURY, M. (eds). 2008. *Mont Terri Rock Laboratory Project, Programme 1996 to 2007 and Results*. Reports of the Swiss Geological Survey, **3**. Swiss Geological Survey, Wabern.

BOSSART, P., MEIER, P.M., MOERI, A., TRICK, T. & MAYOR, J.C. 2002. Geological and hydraulic Characterization of the excavation disturbed zone in the Opalinus Clay of the Mont Terri Rock Laboratory. *Engineering Geology*, **66**, 19–38.

CORKUM, A.G. & MARTIN, C.D. 2007. Modelling a Mine-By test at the Mont Terri rock laboratory, Switzerland. *International Journal of Rock Mechanics and Mining Sciences*, **44**, 846–859, http://doi.org/10.1016/j.ijrmms.2006.12.003

FERRARI, A., FAVERO, V., MANCA, D. & LALOUI, L. 2013. *Geotechnical Characterization of Core Samples from the Geothermal Well Schlattingen SLA-1*. NAGRA Arbeitsbericht NAB 12–50. NAGRA, Wettingen, Switzerland.

FERRARI, A., FAVERO, V., MARSCHALL, P. & LALOUI, L. 2014. Experimental analysis of the water retention behavior of shales. *International Journal of Rock Mechanics and Mining Sciences*, **72**, 61–70.

GEOMECHANICA 2013. *Extent and Shape of the EDZ around Underground Structures of a Geological Repository for Radioactive Waste – A Sensitivity Study for the Candidate Host Rocks in the Proposed Siting Regions in Northern Switzerland*. NAGRA Arbeitsbericht NAB 13–78. NAGRA, Wettingen, Switzerland.

GEOMECHANICA 2014. *HGA Experiment: Numerical Simulation of the EDZ Formation and Mechanical Re-compaction Process Using a FDEM Approach*. Mont Terri Project Technical Note TN 2014-89. Mont Terri Project, St-Ursanne, Switzerland.

HAWKINS, I.R., SWIFT, B.T., HOCH, A.R. & WENDLING, J. 2011. Comparing flows to a tunnel for single porosity, double porosity and discrete fracture representations of the EDZ. *Physics and Chemistry of the Earth*, **36**, 1990–2002.

JACKSON, C.P., HOCH, A.R. & TODMAN, S. 2000. Self-consistency of a heterogeneous continuum porous medium representation of a fractured medium. *Water Resources Research*, **36**, 189.

LANYON, G.W. & SENGER, R. 2011. A structured approach to the derivation of effective properties for combined water and gas flow in the EDZ. *Transport in Porous Media*, **90**, 95–112.

LANYON, G.W., MARSCHALL, P., TRICK, T., DE LA VAISSIÈRE, R., SHAO, H. & LEUNG, H. 2009.

Hydromechanical evolution and self-sealing of damage zones around a microtunnel in a claystone formation of the Swiss Jura Mountains. *In*: *43rd US Rock Mechanics Symposium & 4th US–Canada Rock Mechanics Symposium*, June 28–July 1, 2009, Asheville, North Carolina. American Rock Mechanics Association, Alexandria, VA, 652–663 (paper 09-333).

LANYON, G.W., MARSCHALL, P., TRICK, T., DE LA VAISSIERE, R., SHAO, H. & LEUNG, H. 2014. Self-sealing experiments and gas injection tests in a backfilled microtunnel of the Mont Terri URL. *In*: NORRIS, S., BRUNO, J. *ET AL.* (eds) *Clays in Natural and Engineered Barriers for Radioactive Waste Confinement*. Geological Society, London, Special Publications, **400**, 93–106, http://doi.org/10.1144/SP400.8

LISJAK, A., GARITTE, B., GRASSELLI, G., MÜLLER, H. & VIETOR, T. 2015. The excavation of a circular tunnel in a bedded argillaceous rock (Opalinus Clay): short-term rock mass response and FDEM numerical analysis. *Tunnelling and Underground Space Technology*, **45**, 227–248.

LISJAK, A., TATONE, B.S.A. *ET AL.* 2016. Hybrid finite-discrete element simulation of the EDZ formation and mechanical sealing process around a microtunnel in Opalinus Clay. *Rock Mechanics and Rock Engineering*, **49**, 1849–1873, http://doi.org/10.1007/s00603-015-0847-2

MARSCHALL, P., DISTINGUIN, M., SHAO, H., BOSSART, P., ENACHESCU, C. & TRICK, T. 2006. Creation and evolution of damage zones around a microtunnel in a claystone formation of the Swiss Jura Mountains. Paper SPE-98537 presented at the SPE International Symposium and Exhibition on Formation Damage Control, 15–17 February 2006, Lafayette, LA, USA, http://doi.org/10.2118/98537-MS

MARTIN, C.D. 1997. Seventeenth Canadian Geotechnical Colloquium: the effect of cohesion loss and stress path on brittle rock strength. *Canadian Geotechnical Journal*, **34**, 698–725.

MARTIN, C.D. & LANYON, G.W. WITH CONTRIBUTIONS FROM P. BOSSART & P. BLÜMLING 2003. *EDZ in Clay Shale: Mont Terri*. Mont Terri Technical Report 2001. GeoScience Ltd, Falmouth.

NAGRA 2002. *Projekt Opalinuston – Synthese der geowissenschaftlichen Untersuchungs-ergebnisse. Entsorgungsnachweis für abgebrannte Brennelemente, verglaste hochaktive sowie langlebige mittelaktive Abfälle*. NAGRA Technical Report NTB 02-03. NAGRA (National Cooperative for the Disposal of Radioactive Waste), Wettingen, Switzerland.

NAGRA 2004. *Effects of Post-Disposal Gas Generation in a Repository for Spent Fuel, High-Level Waste and Long-Lived Intermediate Level Waste Sited in Opalinus Clay*. NAGRA Technical Report NTB 04-06. NAGRA (National Cooperative for the Disposal of Radioactive Waste), Wettingen, Switzerland.

NUSSBAUM, C., BOSSART, P., AMANN, F. & AUBOURG, C. 2011. Analysis of tectonic structures and excavation induced fractures in the Opalinus Clay, Mont Terri underground rock laboratory (Switzerland). *Swiss Journal of Geosciences*, **104**, 187–210, http://doi.org/10.1007/s00015-011-0070-4

POLLER, A., SMITH, P., MAYER, G. & HAYEK, M. 2014. *Modelling of Radionuclide Transport along the Underground Access Structures of Deep Geological Repositories*. NAGRA Technischer Bericht NTB 14-10. NAGRA (National Cooperative for the Disposal of Radioactive Waste), Wettingen, Switzerland.

ROMERO, E. & GÓMEZ, R. 2013. *Water and Air Permeability Tests on Deep Core Samples from Schlattingen SLA-1 Borehole*. NAGRA Arbeitsbericht NAB 13-51. NAGRA (National Cooperative for the Disposal of Radioactive Waste), Wettingen, Switzerland.

STEINER, W., KAISER, P.K. & SPAUN, G. 2010. Role of brittle fracture on swelling behaviour of weak rock tunnels: hypothesis and qualitative evidence. *Geomechanics and Tunnelling*, **3**, 583–596.

TSANG, C.F., BERNIER, F. & DAVIES, C. 2005. Geohydromechanical processes in the Excavation Damaged Zone in crystalline rock, rock salt, and indurated and plastic clays – in the context of radioactive waste disposal. *International Journal of Rock Mechanics and Mining Sciences*, **42**, 109–125.

YONG, S. 2008. *A three-dimensional analysis of excavation-induced perturbations in the Opalinus Clay at the Mont Terri Rock Laboratory*. PhD thesis, ETH Zurich.

YONG, S., KAISER, P.K. & LOEW, S. 2010. Influence of tectonic shears on tunnel-induced fracturing. *International Journal of Rock Mechanics and Mining Sciences*, **47**, 984–907.